Int. J. Therm. Sci. (1999) 38, 808–818

An experimental investigation on air impinging jets using visualisation methods

Carlo Carcasci

DEF, Dipartimento di Energetica S. Stecco, University of Florence, via Santa Marta, 3, 50139 Florence, Italy

(Received 20 January 1999, accepted 6 April 1999)

Abstract — Impinging jets are used in many applications for cooling or heating systems, for example cooling gas turbine blades. The jet impact on a surface and the interaction between the jet and the flow determine a complex flow field which leads to a high heat transfer coefficient. The study of this flow field is thus very important. An experimental flow visualisation study has been conducted using several techniques (smoke technique, oil and pigment and the thermotropic liquid crystal technique) to determine the flow pattern for a row and a system of jets impinging on a flat plate with subsonic velocity. Some secondary vortexes are shown, thus allowing the heat transfer coefficient distribution to be understood. © 1999 Éditions scientifiques et médicales Elsevier SAS.

impinging jets / smoke technique / oil pigment technique / liquid crystal technique / flow visualisation / vortexes interaction

Nomenclature

d_j	jet diameter	m
k	thermal conductivity	$W \cdot m^{-1} \cdot K^{-1}$
L	distance between jets	m
Nu	Nusselt number ($Nu = h\, d_j/k$)	
Re_j	jet Reynolds number ($Re_j = u_j\, d_j/v$)	
u_j	jet velocity	$m \cdot s^{-1}$
x	transverse direction	m
z	normal direction, distance between jet and plate	m
ρ	density	$kg \cdot m^{-3}$
μ	dynamic viscosity	Pa·s
v	kinematic viscosity	$m^2 \cdot s^{-1}$

1. INTRODUCTION

The applications of impinging jets are wide-ranging. They are used for heating or cooling in many systems, such as the cooling of electronic components, glass production, and heating for drying textiles. Impingement is also used to cool blades of advanced gas turbines.

Jet impingement on a surface produces a high heat transfer coefficient near the stagnation point. The flow field near the impingement point is very complicated because the jet flow can interact with the flow around itself (*figure 1*), and with the vortices formed by neighbouring jets. Thus, flow field analysis is very important.

Many studies have been carried out of air jets impinging on flat plates, particularly with a single jet. In the present study, the interaction between

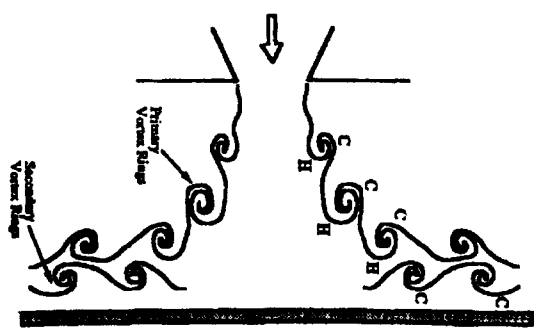

Figure 1. Scheme of some vortexes for a single impinging jet.

* carca@brun.de.unifi.it

impingement jets on flat plate are studied with several experimental flow visualisation techniques (oil and pigment, smoke and thermotropic liquid crystal). Thus, various vortexes can be shown. The aim of the present paper is to compare the results of different visualisation techniques, because each one demonstrates different effects; comparing the results the complete flow field of the impinging jet on a flat plate with and without crossflow can be determined. When the vortexes are described, the effect of vortexes on the flat plate is analysed because these vortexes influence the heat transfer coefficient.

Previous studies

Numerous papers have been written about free jets and jets impinging on a flat plate. Downs and James [7] carried out an extensive literature survey, with a summary of findings. Some research projects have determined the heat transfer coefficient and recovery factor for a single jet and a row of jets impinging on a flat plate. Kieger [11] determined the local and average Nusselt numbers for a single circular jet of air impinging normally on a flat plate and then obtained a correlation to determine the local and average heat transfer coefficient. Goldstein et al. [8] studied the radial distribution of the recovery factor and the local heat transfer for an axial-symmetric impinging air jet and developed a correlation for heat transfer. Goldstein et al. [9] presented the radial distributions of the recovery factor, the effectiveness and local heat transfer coefficient of an air jet impinging on a flat plate and developed a correlation for effectiveness. Obot et al. [13] determined and compared the Nusselt number for a single circular jet of air impinging normally on a flat plate for some different nozzle shapes. Goldstein and Timmers [10] used liquid crystals coated on a mylar sheet to determine the heat transfer coefficient distribution on a flat plate on which either a single jet or an array of jets impinged.

Carcasci and Carnevale [3] used a smoke technique to show the vortex of a free jet and a single impinging jet. Carcasci and Ammannati [4] used some experimental visualisation techniques for a single impinging jet.

Cho et al. [5] determined the heat transfer coefficient of a single impinging jet and showed some figures concerning flow visualisation by the smoke technique, velocity field and turbulence level.

2. TEST APPARATUS

In the present study, smoke techniques, oil and pigment and thermotropic liquid crystal techniques are used, so the experimental apparatus needs to be changed to obtain the best results, because different experimental techniques should be used for different velocities and dimensions.

2.1. Smoke technique

Smoke is injected into the flow field, so that it describes the same flow pattern as the main flow [15]. The smoke can be visualised using a strong light or sheet laser [15]. This is a good technique for studying the flow field for very low speeds, because the best result are obtained when the flow is laminar.

Hardware and procedure

To obtain a Reynolds number ($Re_j = \rho u_j d_j/\mu$) within the range used in gas turbine applications and considering that the jet velocity should be low to obtain good images, jet diameters are large.

The flow pattern is unsteady [3], so a video camera is used to obtain sequential images.

Figure 2 shows the experimental apparatus for the smoke technique. The air is sent into a receiver by a compressor. In the tube, between the compressor and the receiver, there is an orifice meter for the measurement of the air mass flow rate. Using oil, an electric resistance located at the end of a probe produces smoke and is injected into the receiver. The smoke is mixed with the air and this mixture escapes through the jet hole. A glass rod is used to expand the beam from He–Ne laser into a sheet to illuminate cross section slices of the flow, made visible by smoke generation. Photographs of the visualised flow patterns are made using a video camera and can be recorded (*figure 3*).

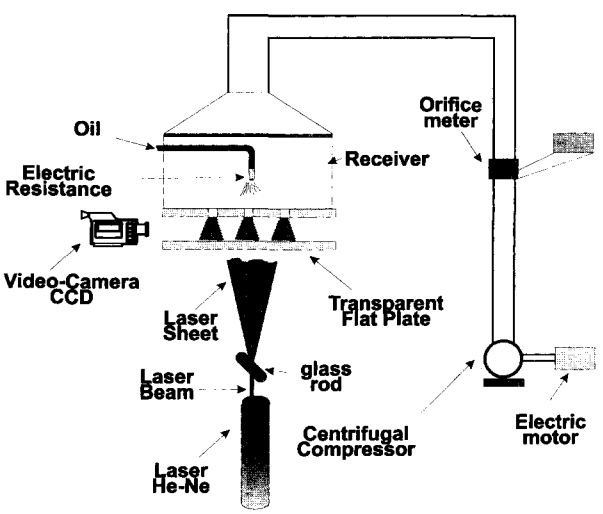

Figure 2. Experimental apparatus for the smoke technique.

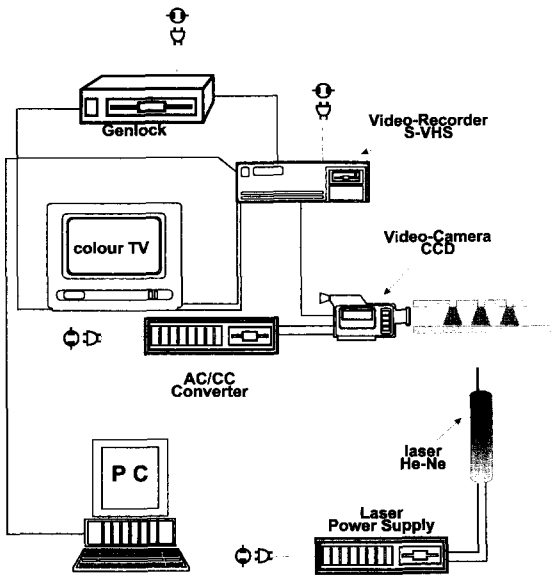

Figure 3. Analog-digital components description used to capture images for the smoke technique.

The images show the vortexes in the volume between the two parallel flat plates; the bottom flat plate is made of transparent material (teflon), so the laser sheet can light up the vortex zone from the lower part. There are some holes on the topmost flat plate, which determine the jets. This surface is black so as to avoid laser reflection. *Figure 4* shows the geometry of holes and volume. The jets are determined by three cylindrical holes (diameter is $d_j = 20$ mm and the thickness is equal to diameter, without chamfering), the distance between the holes is 6 times the diameter ($L/d_j = 6 \Rightarrow L = 120$ mm). The distance between the two surfaces is twice the diameter ($z/d_j = 2 \Rightarrow z = 40$ mm). The experimental apparatus is also modified to allow smoke injection in only one hole.

Euro-Standard video components are used, so images are taken with a frequency of 25 Hz. Consequently the time between two sequential images is 0.04 s. Then, using a PC, the images can be processed with a commercial program changing contrast, brightness or using certain filters.

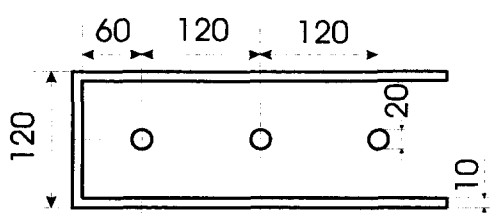

Figure 4. Hole scheme and geometry for the smoke technique.

2.2. Oil and pigment technique

The oil and pigment technique is used to describe the flow field on a surface [15]. This technique can study the flow field for high speeds and can be used at discrete points or as a uniform paint application.

Hardware and procedure

The experimental apparatus of black paint technique differs from the smoke technique because the speed should be higher. So, to obtain a Reynolds number comparable with the smoke technique, the dimensions of the jet diameter d_j are smaller than previous experimental apparatus. *Figure 5* shows the scheme of the holes. Nine holes are made and the distance between the holes are 6 or 12 times the diameter ($L/d_j = 6, 12$). The distance between the flat plate can be 2, 4 or 8 times the diameter ($z/d_j = 2, 4, 8$).

A mixture of oil (motor oil) and pigment is prepared. Their ratio in the mixture depends on the flow speed. Then, contact paper is put on the surface and painted uniformly with the already prepared mixture. The surface is placed (steady pins are used to determine the exact position of bottom flat plate in respect to the topmost one) below the jet for 20–40 min, thus the flow drags the oil with pigment and leaves less pigment in the zones where the shear stress is bigger; so, in this zone, the black intensity is less. The bottom flat plate with the sheet of paper is moved to a bench equipped with a quartz-iodine lamp (*figure 6*). Then the image obtained is captured with a camera and processed on a computer to produce a file, from which the black intensity value in each point of the image can be determined and plotted.

In some studies, the film is not painted uniformly, but with discrete dots, so when the surface is put below the jet, the mixture in each point produces a trace [12].

It should be noted that if the speed is too low, the flow cannot move the mixture and a good result cannot be obtained.

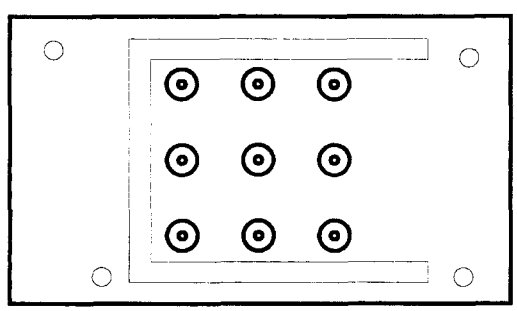

Figure 5. Hole scheme and geometry for the black paint technique.

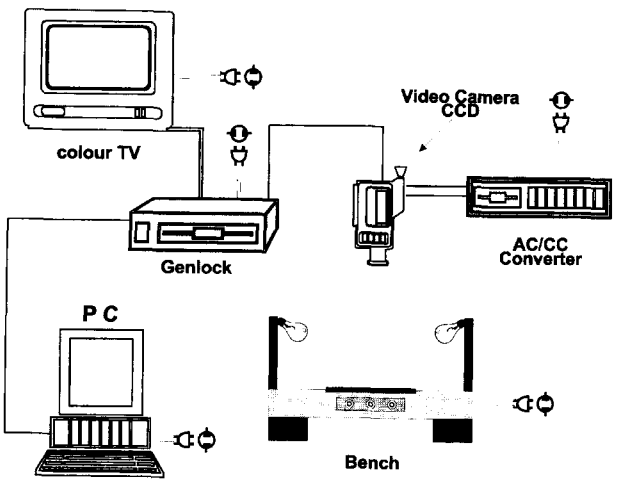

Figure 6. Analog-digital components description used to capture images for the black paint technique.

2.3. Thermotropic liquid crystal

Thermotropic liquid crystal (TLC) behaviour changes according to temperature, as does its colour [15]. Using TLC, the spatial and temporal temperature distribution of a surface can be obtained; so, from the local temperature distribution, the heat transfer coefficient can be determined [15].

Using the analogy between the heat transfer and momentum equations, the heat transfer coefficient can be related to skin friction.

Hardware and procedure

The experimental apparatus is similar to the black paint apparatus, the main difference being in the bottom surface. It consists of three elements (*figure 7*): there is a transparent flat plate (teflon); on which there is a thermotropic liquid crystal sheet (consisting of 4 elements: glue, black layer, TLC and transparent sheet); finally there is a sheet steel (0.05 mm thick) to obtain a higher temperature than that of the impinging air jet. The high temperature is generated by an electric current supplied by a controlled constant-current source.

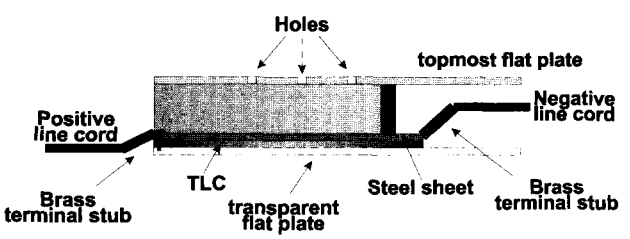

Figure 7. Bottom surface made of 3 elements.

The thermotropic liquid crystals used the range from 29 to 33 °C and cross the following colours: black (33 °C) – blue – green – red – black (29 °C).

The jets impinge on the hot sheet steel, cooling it according to the heat transfer coefficient. Thus, the temperature decrease is visualised by liquid crystals. The images are captured by a CCD colour video camera, placed on the bottom of the transparent flat plate, and are stored in a video recorder. The experimental apparatus is shown in *figure 8*. Finally, the images can be digitised by a PC.

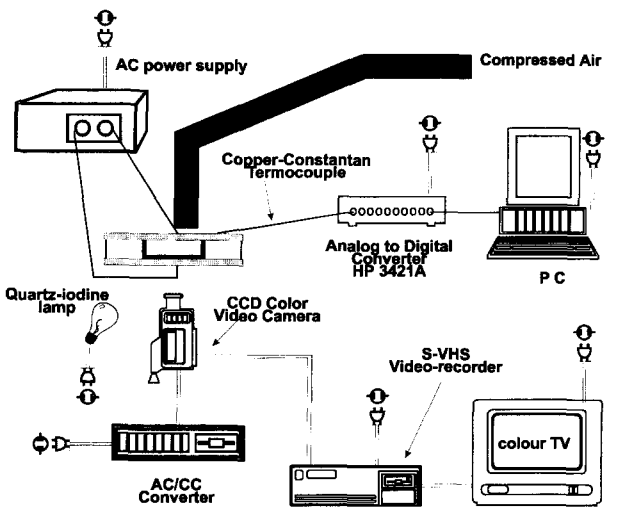

Figure 8. Analog-digital components description used to capture images for thermotropic liquid crystal technique.

3. RESULTS AND DISCUSSION

3.1. Single jet

The aim of this experiment is not to study a single impinging jet, although the latter is fundamental for other effects. *Figure 9* shows a single jet using the smoke technique; on the right-hand side a rising vortex on the free jet impacts on the surface, while another vortex rises upstream. Thus, the phenomenon is unsteady. Therefore, a video camera is needed to study these vortexes.

The vortexes have a ring shape, so, when the nozzle is close to surface (z/d_j is small), the highest effect of the impinging jet on the surface is not at the centre line, but in a ring around it. *Figure 10* shows the image and the black intensity level of a single jet. Two clear peaks around the centre-line are found with a minimum at the centre-line. Cho et al. [5] found a minimum of Nusselt number on the centre-line for a small jet height.

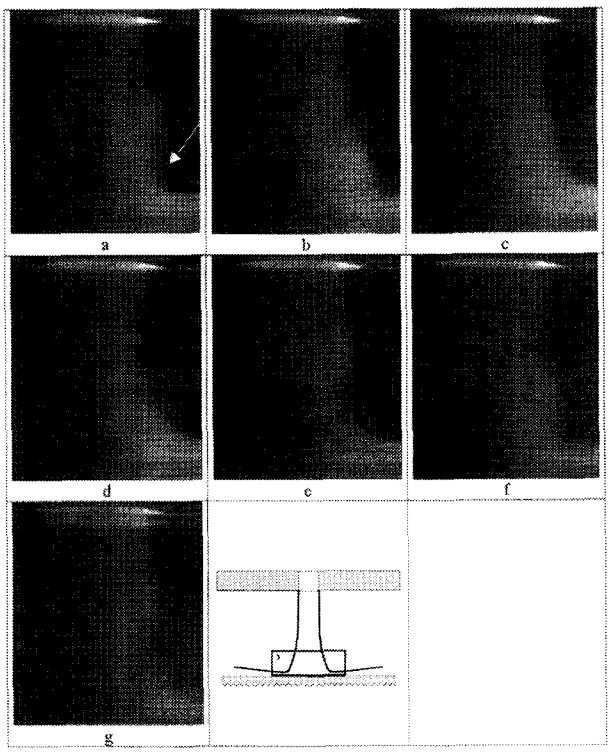

Figure 9. Visualisation of a single jet using the smoke technique.

The maximum value of Nusselt number is located at about $x/d_j = 0.6$ [5], similar to the black intensity result determined by *figure 10*. The velocity near the surface accelerates at about $x/d_j = 0.6$; this acceleration decreases the boundary layer thickness.

3.2. Interaction of inline jets

The jets with the ring-vortexes move in the stream wise direction dragged by the jet as far as the plate, where it impinges on the plate changing shape and continues in an x-direction (on flat plate). When it arrives at the point where the jet meets the jet of the next nozzle, the flow goes upward and there is a large vortex (*main vortex*; *figure 11*).

Figure 12 shows the interaction between two impinging jets in the meeting zone. In this zone, the *main vortex* meets the *main vortex* of the nearby jet and two small adverse vortexes (*lower adverse vortexes*) are generated.

Figure 13 shows the interaction between two impinging jets in the high meeting zone. Two adverse vortexes (*upper adverse vortexes*) are also generated in this region by interaction of *main vortexes* and upper flat plate.

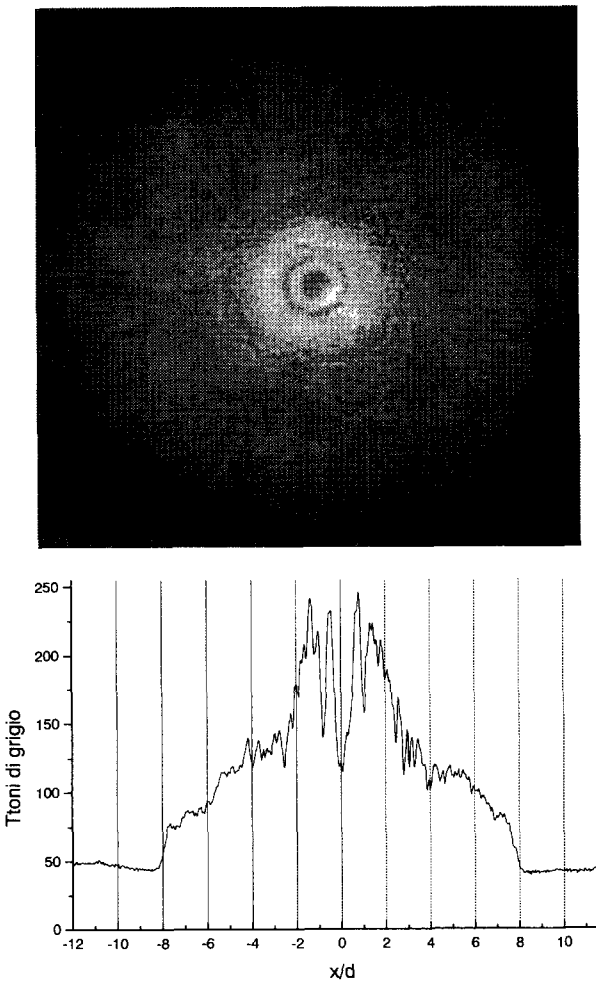

Figure 10. Image and black intensity level of a single jet ($d_j = 2$ mm, $z/d_j = 2$, $Re_j = 50\ 000$).

Figure 14 shows the scheme of vortexes generated by impinging jet interaction. This one is an interpretation of the previous visualisation results.

3.3. Interaction of inline jets with crossflow

The interaction of impinging jets with crossflow is shown in *figure 15*. The crossflow comes from the left-hand side to the right hand side. The *lower adverse vortexes* do not change their position significantly, but the *main vortexes* and the *upper adverse vortexes* change because the crossflow drags them downstream. So, the *main vortex* and the *upper adverse vortex* of the upstream impinging jet overhang the vortexes of the downstream impinging jet; therefore these vortexes are smaller than in the case without crossflow.

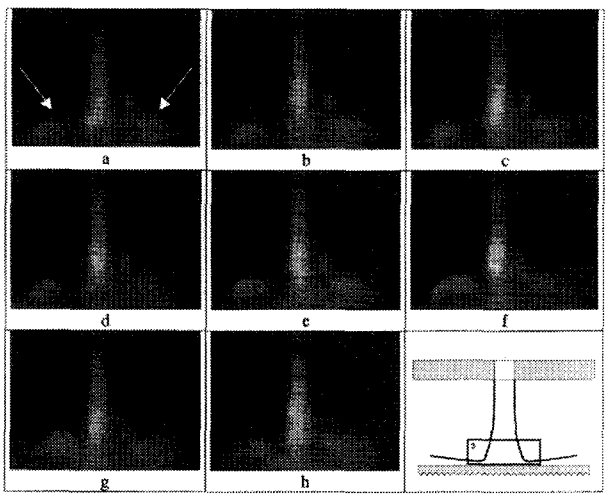

Figure 11. Visualisation of the main vortex on the impinging zone.

Figure 16 shows the scheme of the interaction of impinging jets with crossflow; this is an interpretation of the previous visualisation results.

3.4. Interaction of 9 jets with crossflow

Figures 17, *18* and *19* show the results of 9 impinging jets with crossflow (the crossflow comes from the top to the bottom of images) using the black paint technique. The figures are for different distances of the jet holes to flat plate ($z/d_j = 2, 4, 8$).

In all figures, the tracks of the *lower adverse vortexes* are clear. They have an approximately quadrangle shape. At the point where the *lower adverse vortexes* meet the others, the phenomenon is not clear because oil with black pigment accumulates and the tracks cannot be seen. This means that the *lower adverse vortexes* of a jet go in two opposite directions, taking the oil as far as the point where it meets the other vortexes. Probably, at this point, the *lower adverse vortexes* of all jets go upward. However, the *lower adverse vortexes* do not feel the effect of crossflow.

Figure 17, the case with the smallest distance between the flat plate, shows a double ring around the centre line of each jet, like the case of a single jet (*figure 10*); the double ring of the last jets, where the crossflow is stronger, are not symmetric and the external ring becomes a semi-ring. In the case of vortexes upstream of centre line, where the impinging flow is adverse to the crossflow, the crossflow goes above the vortexes, which, consequently, increases the skin friction with the surface. On the other hand, with the vortexes downstream of centre line, where the impinging flow

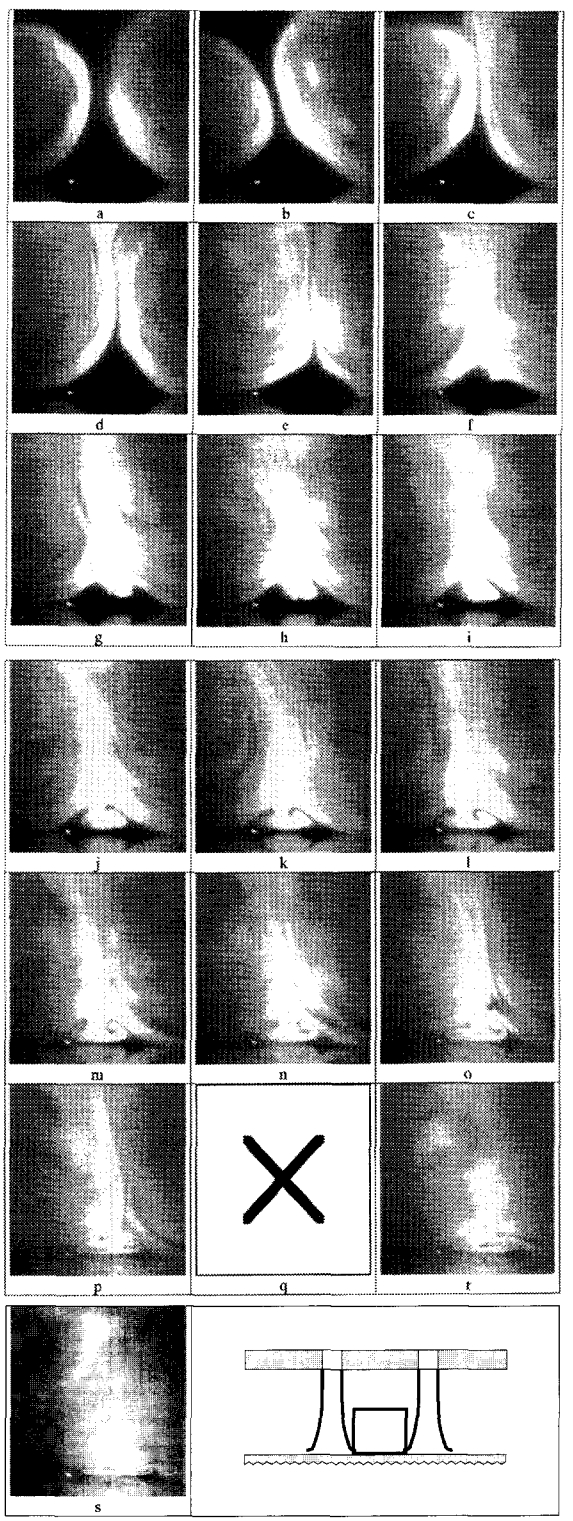

Figure 12. Visualisation of the interaction of the main vortex in the lower meeting zone.

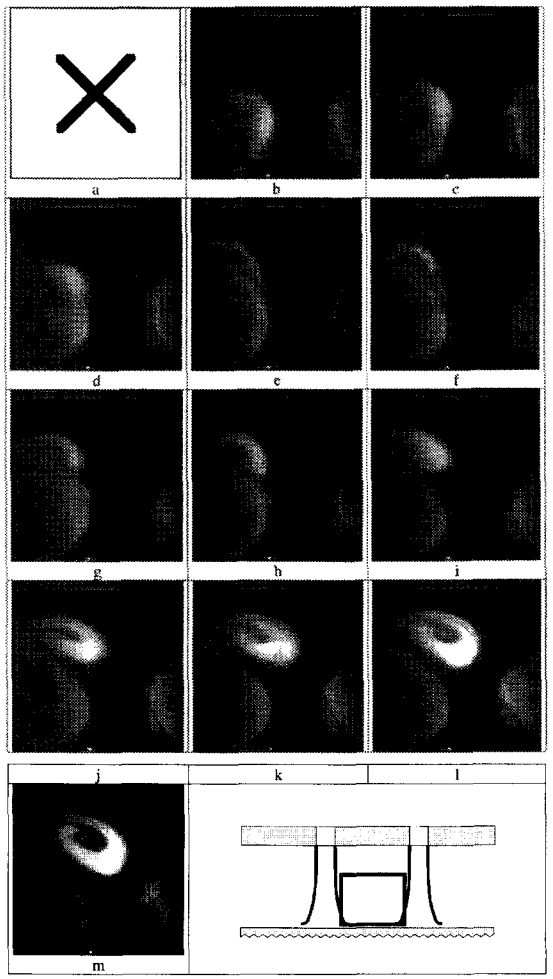

Figure 13. Visualisation of the interaction of the main vortex in the upper meeting zone.

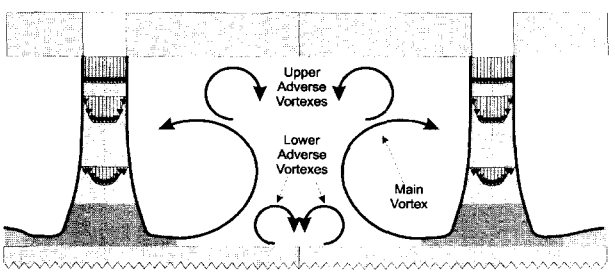

Figure 14. Scheme of vortexes of the interaction of two impinging jets.

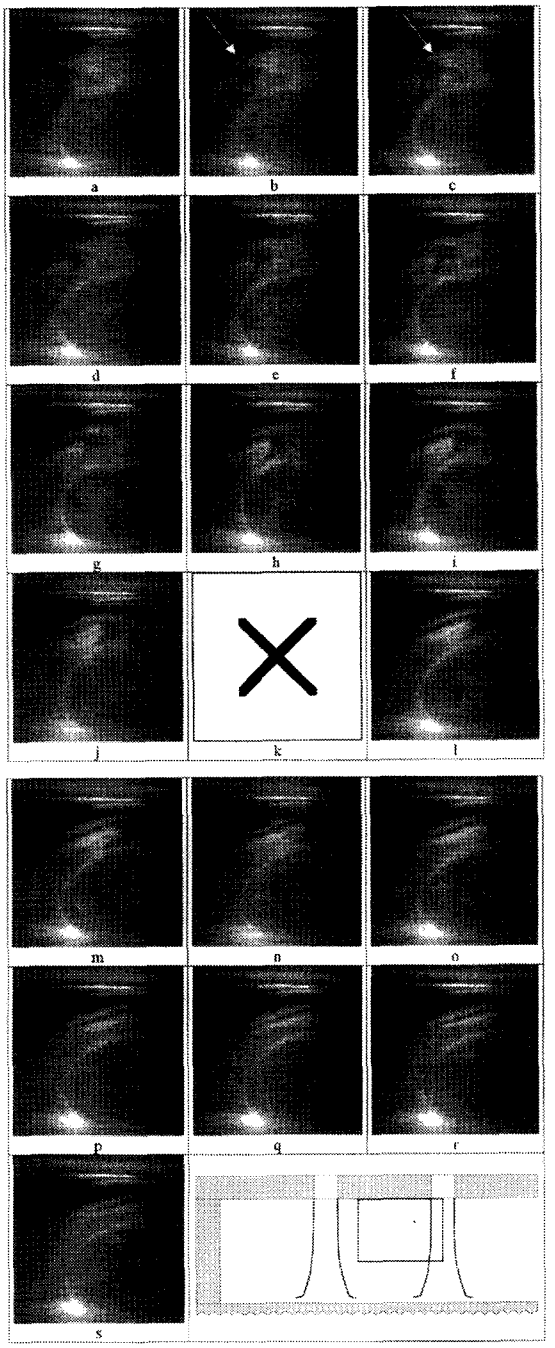

Figure 15. Visualisation of the interaction of the main vortex in the meeting zone with crossflow.

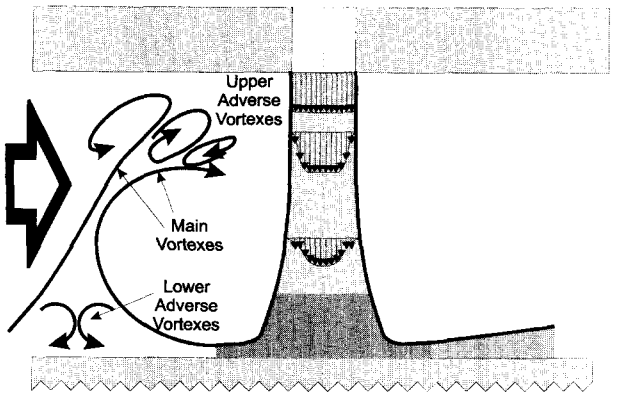

Figure 16. Scheme of vortexes of the interaction of 2 impinging jets with crossflow.

is in agreement with the crossflow, the crossflow drags the impinging flow, so the vortexes are less strong. *Figure 20*, using the discrete dot oil and paint pigment, allows this phenomenon to be better understood.

Comparing *figure 17* with *figures 18* and *19*, a different black intensity at the centre line can be noted. In the case with a small z/d_j (*figure 17*) a double ring can be clearly seen; when the distance between the surfaces (z/d_j) is increased, the rings are initially unclear (*figure 18*), then disappear completely (*figure 19*).

Figures 21 and *22* show the images and the black intensity of 9 impinging jets with crossflow, with a bigger distance between the jets ($L/d_j = 12$). Comparing these images with the previous ones (*figure 21* versus *figure 17* and *figure 22* versus *figure 18*), the rings around centre line are present in both cases, but in the cases with a larger distance between the jets (*figures 21* and *22*), the rings are symmetric because the crossflow is less strong. Moreover, the tracks of *lower adverse vortexes* are no longer present because they are less strong.

Figure 23 shows the images obtained using thermotropic liquid crystals. In these images, the ring around centre line is clear. The effect of *lower adverse vortexes* is less evident.

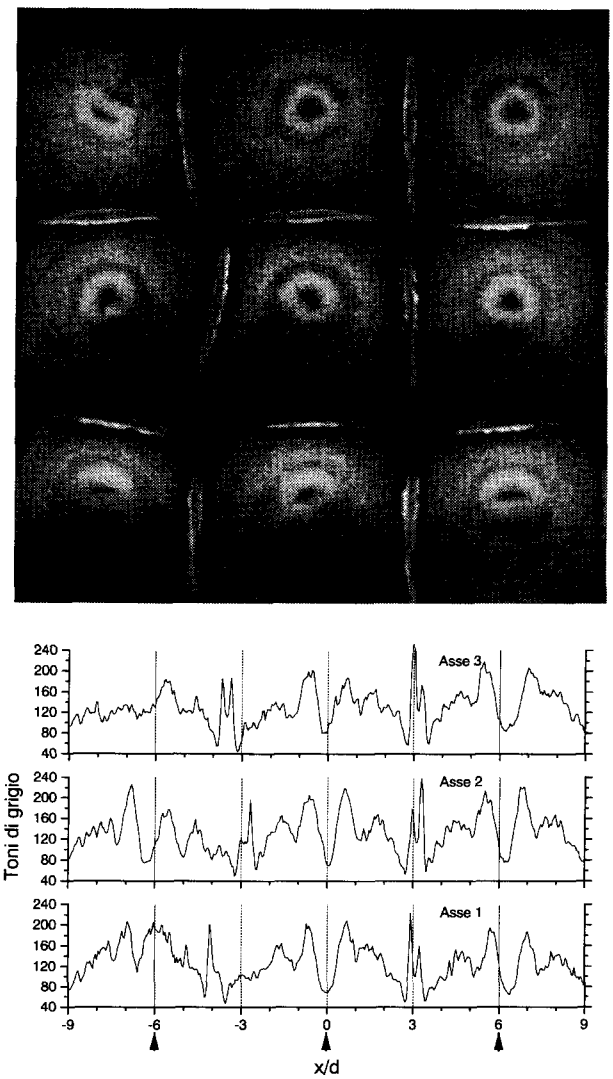

Figure 17. Image and black intensity level of 9 jets with crossflow ($d_j = 2$ mm, $z/d_j = 2$, $L/d_j = 6$, $Re_j = 50\,000$).

4. CONCLUSIONS

The interaction between impinging jets generated by a hole in a flat plate on another flat plate are analysed using several experimental techniques (smoke technique, oil paint technique and thermocropic liquid crystal).

A ring vortex around centre line is generated by the interaction of a free jet and the neighbouring flow. When the distance between the surfaces is small and the Reynolds number high, this ring vortex determines a high heat transfer coefficient around the stagnation point on the flat plate. Subsequently, the impinging flow determines a *main vortex*, and when it interacts with the *main vortex* of another jet, two vortexes are generated in the space between the *main vortexes* and the bottom flat plate (*lower adverse vortexes*). They are important because they determine a local peak of heat transfer coefficient. The interaction between the *main vortexes* and the topmost flat plate (where jet holes are situated) determines a second series of vortexes (*upper adverse vortexes*). The phenomenon is unsteady, so a video camera is necessary to understand it better.

When a crossflow is present, the *lower adverse vortexes* are not particularly influenced, while the *upper adverse vortexes* are dragged by crossflow. The ring vortexes are influenced by crossflow.

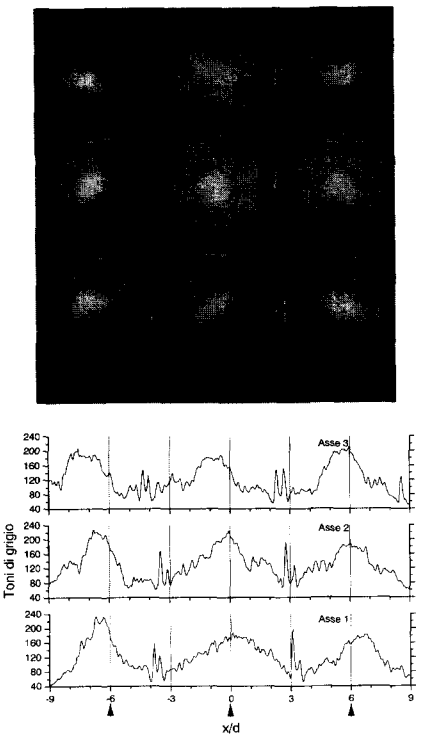

Figure 18. Image and black intensity level of 9 jets with crossflow ($d_j = 2$ mm, $z/d_j = 4$, $L/d_j = 6$, $Re_j = 50\,000$).

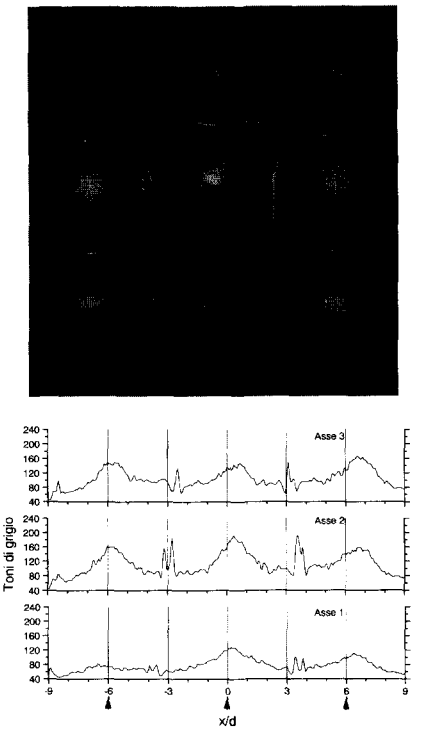

Figure 19. Image and black intensity level of 9 jets with crossflow ($d_j = 2$ mm, $z/d_j = 8$, $L/d_j = 6$, $Re_j = 50\,000$).

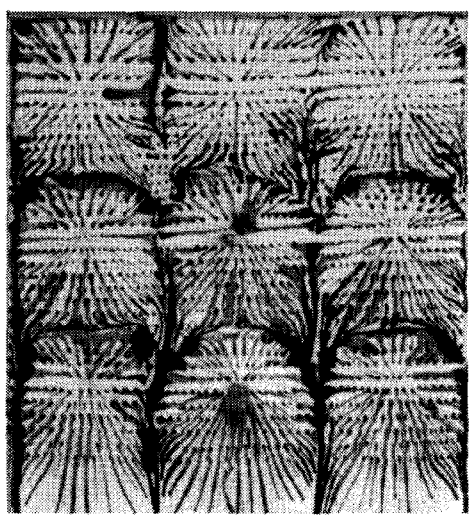

Figure 20. Discrete dot oil and paint pigment of 9 jets with crossflow ($d_j = 2$ mm, $z/d_j = 8$, $L/d_j = 6$, $Re_j = 10\,000$).

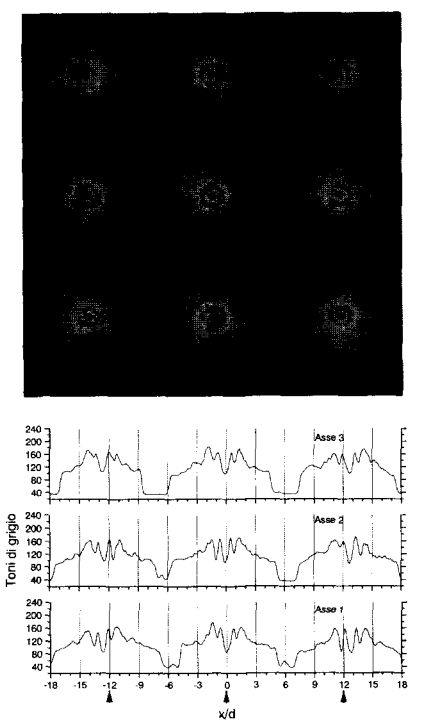

Figure 21. Image and black intensity level of 9 jets with crossflow ($d_j = 2$ mm, $z/d_j = 2$, $L/d_j = 6$, $Re_j = 10\,000$).

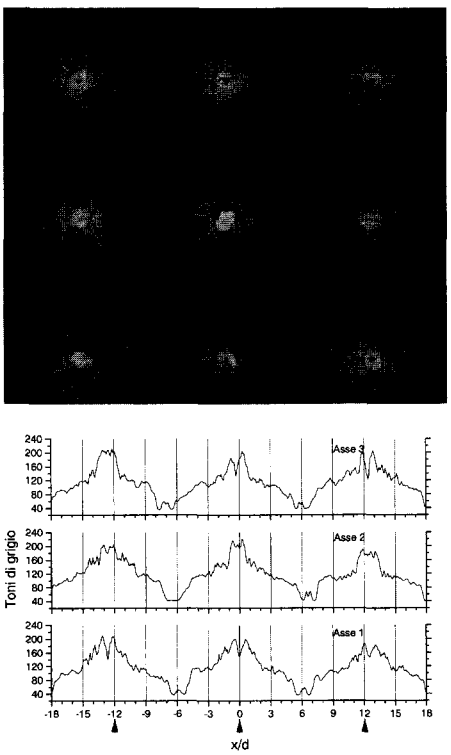

Figure 22. Image and black intensity level of 9 jets with crossflow ($d_j = 2$ mm, $z/d_j = 4$, $L/d_j = 12$, $Re_j = 50\,000$).

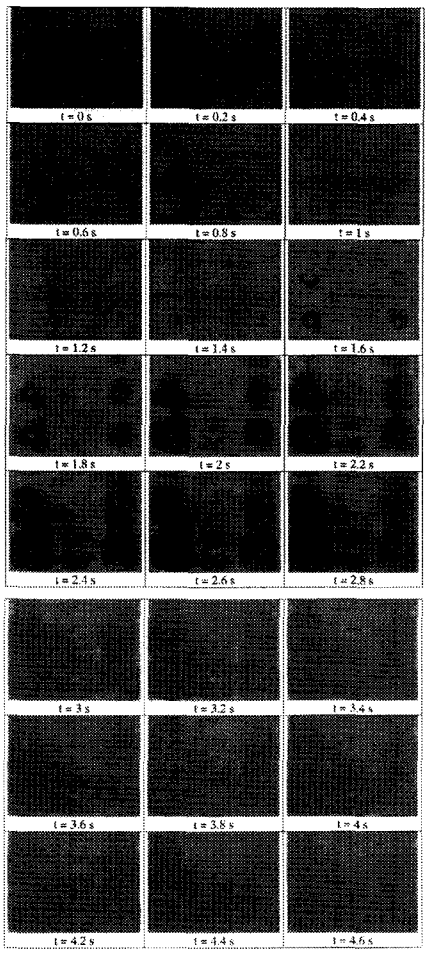

Figure 23. Image of 9 jets with crossflow ($d_j = 2$ mm, $z/d_j = 4$, $L/d_j = 6$, $Re_j = 50\,000$) using the thermocropic liquid crystal technique.

Acknowledgements

The author would like to thank Prof. E. Carnevale, Prof. M. De Lucia and Dr. A. Ammannati for their valuable contributions to this study. The authors would also like to thank MURST (Italian Ministry for Universities) for its financial support.

REFERENCES

[1] Ajersch P., Zhou J.M., Ketler S., Salcudean M., Gartshore I.S., Multiple jets in a crossflow: detailed measurements and numerical simulation, IGTI-Turbo Expo'95, Houston (TX), 4–6 June 1995, 95-GT-9

[2] Behbahani A.I., Goldstein R.J., Local heat transfer to staggered arrays of impinging circular air jets, ASME J. Eng. Power 105 (1983) 354–360.

[3] Carcasci C., Carnevale E., Refrigerazione a Getto delle Palette delle Turbine a Gas: una Nuova Tecnica di Indagine Sperimentale, in: 51° Congresso Nazionale ATI, Udine, 16–20 September 1996, pp. 1323–1332.

[4] Carcasci C. Ammannati A., Analisi qualitativa e visualizzazione del sistema di raffreddamento a getti, in: Giornata Nazionale di Studio MIS-MAC VI, Genova, 2 July 1999.

[5] Cho H.H., Lee C. H., Kim Y.S., Characteristics of heat transfer in impinging jets by control of vortex pairing, in: IGTI Turbo Expo'98, Stockholm (Sweden), June 1998, 98-GT-216.

[6] Douglas Barlow N., Kim Y.W., Transient liquid crystal technique for convective heat transfer on rough surfaces, in: IGTI - Turbo Expo'95, Houston (TX), 4–6 June 1995, 95-GT-6.

[7] Downs S.J., James E.H., Jet impingement heat transfer. A Literature Survey, ASME Paper No. 87-HT-35, 1987.

[8] Goldstein R.J., Behbahani A.I., Kieger Heppelmann K., Streamwise distribution of the recovery factor and the local heat transfer coefficient to an impinging circular air jet, J. Heat Mass Tran. 29 (8) (1986) 1227–1235.

[9] Goldstein R.J., Seol W.S., Heat transfer to a row of impinging circular air jets including the effect of entrainment, J. Heat Mass Tran. 14 (8) (1991) 2133–2147.

[10] Goldstein R.J., Timmers J.F., Visualization of heat transfer from arrays of impinging jets, J. Heat Mass Tran. 25 (12) (1982) 1857-1868.

[11] Kieger K.K., Local and average heat transfer from a flat surface to a single circular jet of air impinging on it, Thesis, University of Minnesota, Mechanical Engineering Department, 1981.

[12] Langston L.S., Boyle M.T., A new surface-streamline flow-visualization technique, Int. J. Heat Mass Tran. 125 (1982) 53-57.

[13] Obot N.T., Majumdar A.S., Douglas W.J.M., The effect of nozzle geometry on impingement heat transfer under a round turbulent jet, ASME paper 79-WA/HT-53, 1979.

[14] Van Treuren K.W., Wang Z., Ireland P.T., Jones T.V., Kohler S.T., Local heat transfer coefficient and adiabatic wall temperature measurement beneath arrays of staggered and inline impinging jets, in: IGTI - Turbo Expo'94, The Hague, Netherlands, 13-16 June 1994, 94-GT-181.

[15] Wen-Jei Yang, Handbook of flow visualization, Taylor & Francis, 1989, pp. 29-38, 41-63, 91-103, 105-124